Forensic gemmological study of green-coloured beryl of variable origin

Jana Fridrichová[1], Peter Bačík[1], Ľudmila Illášová[2], Ján Štubňa[2], Radek Škoda[3], Stanislava Milovská[4]

[1] Comenius University in Bratislava, Faculty of Natural Sciences, Department of Mineralogy and Petrology, Ilkovičova 6, 842 15 Bratislava, Slovakia, jana.fridrichova@uniba.sk
[2] Constantine the Philosopher University in Nitra, Faculty of Natural Sciences, Gemmological Institute, Nábrežie mládeže 91, 949 74 Nitra, Slovakia
[3] Masaryk University, Department of Geological Sciences, Kotlářská 2, 611 37 Brno, Czech Republic
[4] Earth Science Institute of the Slovak Academy of Science, Ďumbierska 1, 974 01 Banská Bystrica, Slovakia

AGEOS

Abstract: Fourteen gem-quality green-coloured beryl samples of different origin were investigated by standard gemmological methods and Raman, X-ray fluorescence and optical absorption spectroscopy. All investigated 14 samples were identified as beryl by Raman spectroscopy. Five main transition elements were detected (Cr, V, Fe, Cu, Ni). Six samples were significantly enriched in Cr. These samples also had the highest luminescence at about 685 and 680 nm corresponding to R_1 and R_2 bands which is good identification factor for emeralds. Two of these samples were also enriched in vanadium. In two other Cr-rich samples is also Ni and Cu present. These two samples contain also the highest amount of Fe, while the other samples contain lower amounts of Fe. In two of the Fe-bearing samples Cr was not detected. Varying amounts of water inclusions, both type I and II, were detected in each of the samples, except the two Ni- and Cu-bearing samples, which exhibit only H_2O type I. While the samples with a high Cr content were assigned to emerald, the green Fe-rich samples (without Cr) can be named just as green beryl. It seems that a special Cr-V-Fe ratio is indicative for samples, which were found in Colombia. The other samples (except the Ni- and Cu-bearing samples) are likely from various schist-type emerald deposits. There are indications that the two Cu- and Ni-bearing samples with only water type I are Russian hydrothermal syntheses.
Keywords: Raman spectroscopy, chromophore, optical absorption spectroscopy, XRF, gemmology, green-coloured beryl

1. INTRODUCTION

Green-coloured beryl is the most commonly known as emerald. It has been among the most appreciated and desired gemstones since the ancient history. In the business sector, a wide range of green-coloured beryl from variable localities as well as synthetic substitutes is now available. However, not all green-coloured beryl samples are emeralds.

Beryl, $Be_3Al_2Si_6O_{18}$, is a cyclosilicate mineral. Its hexagonal crystal structure consists of Al^{3+} ions octahedrally coordinated by six oxygens and Si^{4+} and Be^{2+} ions tetrahedrally coordinated by four oxygens. Stacked hexagonal rings of $(SiO_4)^{4-}$ tetrahedra are forming channels lying in planes parallel to the crystallographic *c* axis. Rings of SiO_4 tetrahedra are connected with Al octahedral and Be tetrahedral sites and together form beryl crystal structure as a 3D framework. Octahedral Al^{3+} is usually substituted by Fe^{2+}, Fe^{3+}, V^{3+}, Cr^{3+} and other *d* elements. Beryllium in tetrahedron is substituted mainly by Li^+. Heterovalent substitutions are charge-balanced by alkali such as Na^+, K^+, Rb^+, and Cs^+ entering to the channel interstices (Aurisicchio et al., 1988).

According to the Confédération Internationale de la Bijouterie, Joaillerie et Orfèvrerie (CIBJO) regulations, also known as the World Jewellery Confederation, term "emerald" can be used for green beryl containing Cr and/or V. Green-coloured beryl containing Fe is termed green beryl. Gemmological laboratories determine the origin of green-coloured beryl using several, complementary tools that include chiefly observation of microscopic features using binocular microscope (aspect and nature of inclusions; colour zonation), chemical composition measurements (minor and trace elements, e.g., Schwarz, 1991; oxygen isotopes, e.g., Giuliani et al., 1998), and several spectroscopic measurements including infrared absorption spectroscopy (e.g., Stockton, 1987) and optical absorption spectroscopy (e.g., Saeseaw et al., 2014 and references therein).

The aim of this study is to investigate the origin of various green-coloured beryl samples in detail using crystal-chemical properties. Studied samples were obtained from commercial sources with partly declared origin (usually only country of origin). However, in our research, we used gemmological and spectroscopic (Raman, optical absorption, X-ray fluorescence spectroscopy) methods to verify the origin as was provided by the retailers.

2. MATERIALS AND METHODS

We studied 14 green-coloured beryl samples gained from the commercial sources. The seller declared following countries of origin (abbreviations are shown in the brackets): Afghanistan (sample B1), Brazil (B2-B6), Colombia (B7-B8), Russia (B9-B10), Zambia (B11-B12). Two stones had undetermined origin (B13-B14). Most of the samples were cut gemstones of various shapes except B6, B9, B10, B12, B13 samples which were crystal fragments of gemmological quality. Samples were not treated for further analyses.

Standard gemological properties were measured in the Gemmological Institute of Constantine the Philosopher University, Nitra with a refractometer with monochromator filter, polariscope, a Chelsea filter, a synthetic emerald filter set, and four-watt long-wave (365 nm) and short-wave (254 nm) UV lamps to observe fluorescence. The specific gravity measurement was acquired with hydrostatic scales KERN ABT-5DM with extension KERN ABT-A015. Microscopic examination was performed with Motic GM-171 trinocular microscopes at 10×–50× magnification, using both darkfield and brightfield illumination.

Manuscript received 2018-9-27
Revised version accepted 2018-11-22

Raman analyses were performed on the LabRAM-HR Evolution (Horiba Jobin-Yvon) spectrometer system with a Peltier cooled CCD detector and Olympus BX-41 microscope (Masaryk University, Department of Geological Sciences). Raman spectra were excited by two types of lasers and a silicon wafer (520.6 cm^{-1}) was used for spectral calibration. Blue diode laser (473 nm) was used for obtaining Raman spectra in the range of 50-4000 cm^{-1} were collected from each crystal using 50 × objective. The acquisition time of 10 s per frame and 2 accumulations were used to improve signal-to-noise ratio. Green Nd:YAG (532 nm) laser was used for obtaining luminescence spectra in the range of 535-1137 nm from each crystal using 50 × objective. The acquisition

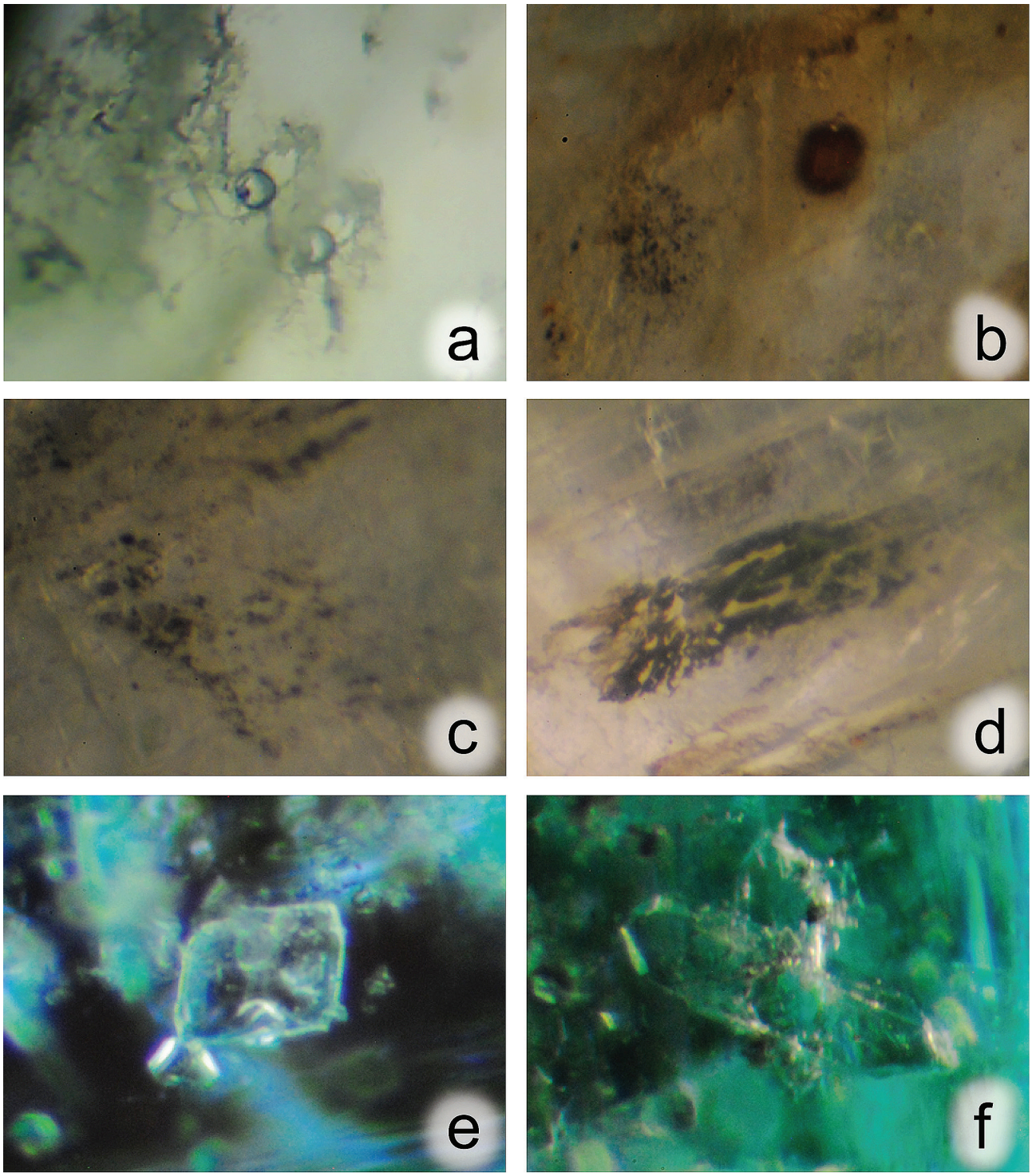

Fig. 1. Fluid and mineral inclusions in studied samples: a) B1 sample – two-phase inclusion (100x magnification); b) B3 sample – phlogopite mineral inclusion (50x); c) B3 sample – magnetite and chromite mineral inclusions (50x); d) B4 sample – ilmenite mineral inclusion (50x); e) B7 sample – calcite mineral inclusion (50x); f) B8 sample – quartz mineral inclusion (50x).

time of 3 s per frame and 2 accumulations were used to improve signal-to-noise ratio.

Optical absorption spectra of cut stones in the region (400–750 nm) were measured with the GL Gem Spectrometer™ at room temperature in the Gemological Institute of Constantine the Philosopher University, Nitra. Both Raman and UV/Vis/NIR spectra were processed in Seasolve PeakFit 4.1.12 software. Raman and absorption bands were fitted by Lorentz function with the automatic background correction and Savitsky-Golay smoothing.

Chemical composition was determined by micro X-ray fluorescence spectroscopy (micro-XRF) using an instrument M4 TORNADO, Bruker (Earth Science Institute of the Slovak Academy of Science, Banská Bystrica). Incident X-ray beam (Rh anode) was focused by polycapillary optics to 25 micron spot, interaction depth was ca. 10-1000 μm, excitation current 600 μA at 50 kV. Analyses were acquired at 20 mBar vacuum. A silicon drift detector (SDD) collecting the fluorescence signal has an active area 30 mm^2 and spectral resolution 145 e. Measuring time of point analyses was 70 s, live time 60 s, energy range of 0.25-20 keV. Element concentrations were computed by fundamental parameters method. Since during analysis no standards were used and beryl contains immeasurable elements, analyses were normalized on basis of SiO_2 = 67 wt %. Despite of the normalization, the analyses were not stoichiometric and the content of several elements was increased inconsistently with the beryl formula. Therefore, we present chemical composition in wt % of selected oxides.

3. RESULTS

The samples` gemmological properties are summarized in Tab. 1. The refractive indices (RI) varied from 1.560 to 1.590, with birefringence between 0.005 and 0.010. Sample B8 had the lowest RI among all samples. The most samples were inert under Chelsea filter observation, but several beryl samples (B7, B8, B10-B12) displayed a particularly strong pink reaction. Synthetic emerald „support" filter set was also used for better identification and only two samples (B13 and B14) showed green-blue colour, the others were inert. The B4 sample revealed green luminescence under 365 nm UV light.

In the microscopic observation, fluid and also mineral inclusions were found (Fig. 1–2). In the B1-B6 samples, two-phase (liquid and vapour) fluid inclusions (Fig. 1a) and moreover,

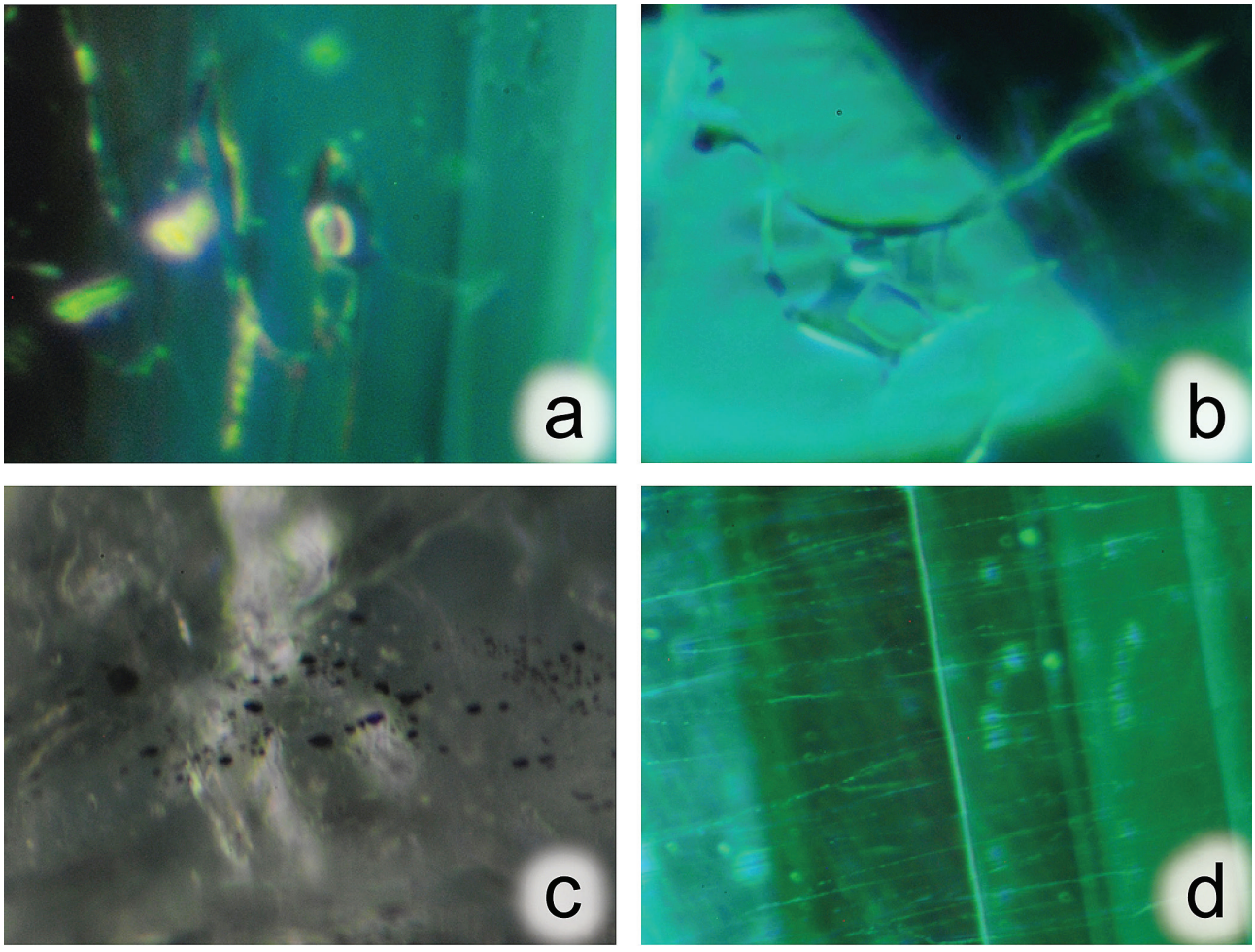

Fig. 2. Fluid and mineral inclusions in studied samples: a) B7 sample – three-phase inclusion (50x magnification); b) B8 sample – three-phase inclusion (50x); c) B11 sample – magnetite mineral inclusions (50x); d) B14 sample – flux particles (20x).

Tab. 1. Gemmological properties of the studied samples.

Sample	B1	B2	B3	B4	B5	B6	B7
Measurements (mm)	5.75x3.64x1.89	5.06x3.81x2.14	4.96x4.07x2.17	5.01x4.00x2.29	5.10x3.90x1.85	18.76x6.44x4.91	5.81x2.59x1.68
Weight (ct)	0.23	0.32	0.34	0.36	0.29	4.86	0.21
Specific Gravity	2.73	2.72	2.68	2.69	2.71	2.67	2.74
Refractive Index	1.56-1.59	1.57-1.58	1.57-1.58	1.57	1.57	unobserved	1.57-1.59
Birefringence	0.01	unobserved	unobserved	unobserved	unobserved	unobserved	unobserved
Pleochroism	Green-blue green	Green-blue green	Green-blue green	Green-blue green	Green-blue green	Green-blue green	Green-blue green
Luminiscence 365 nm	None	None	None	Green	None	None	None
Luminiscence 254 nm	None	None	None	None	None	None	None
Chelsea filter	Inert	Inert	Inert	Inert	Inert	Inert	Pink
Synthetic emerald „support" filter	Inert	Inert	Inert	Inert	Inert	Inert	Inert

Sample	B1	B2	B3	B4	B5	B6	B7
Measurements (mm)	4.31x2.85x2.05	4.86x7.09x5.44	23.01x10.88x9.29	7.12x5.83x4.64	7.14x4.26x3.55	25.55x11.92x7.28	8.29x3.55x2.37
Weight (ct)	0.13	1.17	17.66	1.41	0.79	22.93	0.56
Specific Gravity	2.73	2.67	2.75	2.7	2.73	2.68	2.7
Refractive Index	1.56-1.57	unobserved	unobserved	1.57-1.58	1.58	1.58	1.58
Birefringence	unobserved	unobserved	unobserved	0.005	unobserved	unobserved	0.005
Pleochroism	Green-blue green	unobserved	Green-blue green	Green-blue green	Green-blue green	Green-blue green	Green-blue green
Luminiscence 365 nm	None	None	None	None	None	None	None
Luminiscence 254 nm	None	None	None	None	None	None	None
Chelsea filter	Pink	Inert	Pink	Pink	Pink	Inert	Inert
Synthetic emerald „support" filter	Inert	Inert	Inert	Inert	Inert	Green-blue	Green-blue

mineral inclusions including phlogopite, magnetite, chromite, ilmenite were observed (Fig. 1b–d). Calcite and quartz mineral inclusions (Fig. 1e–f) and three-phase (solid, liquid and vapour) fluid inclusions were detected in the B7, B8 samples (Fig. 2a–b). Fluid and mineral (magnetite) inclusions (Fig. 2c) in the B9–B12 samples were similar to those encountered in B1–B6. Flux patterns were observed in the B14 sample (Fig. 2d).

All the samples were identified by Raman spectroscopy as beryl. Spectra (Fig. 3–5, Tab. 2) were measured only on cut stones and irregular fragments; therefore, measurement orientation is random. Raman spectra ranged from 100 to 1200 cm^{-1} in all samples were very similar. The bands assigned to both water types are very different within each of the samples. Raman spectra also differ by the absence of some vibrations, depending on the random sample orientation to the laser beam. The bands in the range of 3606 – 3607 cm^{-1} are assigned to the ν_1 vibration of H_2O type I and those in the range of 3594–3598 cm^{-1} are associated with ν_1 vibration of H_2O type II. Both bands were present in most of the samples except B13, B14 samples with only H_2O type I. Vibrations ν_2 and ν_3 for both water types are absent.

Luminescence spectra involve R_1 and R_2 bands at about 685 and 680 nm and wider band in the range of 715–748 nm. All the samples exhibit significant luminescence except B6 and B9 samples (Fig. 6–8). The highest luminescence was observed in B3, B7, B8 and B11 samples.

In the XRF chemical analysis, five main chromophores were confirmed in studied samples (Tab. 3). Significant Cr content was detected almost in all samples except B6 and B9. The highest Cr content was determined in the B4, B7, B8 B10, B13, B14 stones. The B7 and B8 samples are, in addition, enriched in vanadium in contrast to all other samples (Fig. 9). All the samples contain Fe; the highest contents were shown in the B13, B14 samples. The other samples are also enriched in Fe but not to such large extent. The increased Fe content is in B1, B2, B6, B10 samples. Moreover, in B13 and B14 samples, Ni and Cu are also present.

Based on the optical absorption spectra (Figs. 10–12, Tab. 4), studied samples can be divided into several groups. First group including B1, B11 and B12 samples (Figs. 10–11) has relatively distinctive band at 430-440 nm assigned according to Tanabe-Sugano diagram to dominant $^4A_{2g} \rightarrow {}^4T_{2g}$ transition in Cr^{3+}. The second $^4A_{2g} \rightarrow {}^4T_{1g}$ transition in Cr^{3+} at 605–616 nm but it

Tab. 2. Raman shifts (cm^{-1}) of Raman-active bands in the studied samples. Assignment of band modes was made according to references (ref.).

		Ref.	B1	B2	B3	B4	B5	B6	B7	B8	B9	B10	B11	B12	B13	B14
A_{1g}	ring	1		323	320	322	320	320	321	321	323	322	321	321	318	319
	ring	1	400	397	393	396	394	394	396	395	397	396	398	398	393	393
	ring	1		615	619	619		622			613	621				
	ring	1	687	686	682	685	686	683	685	684	687	685	685	686	681	681
	Si-O	1, 2	1076	1069	1065	1068	1069	1067	1068	1067	1067	1067	1070	1074	1066	1066
	Si-O	1		1129						1128	1124	1141				
E_{1g}	ring	1		519	521	523	523	526	523	524	519	526		519	522	522
	Si-O	3						918								
	Si-O	1		1012	1009	1013	1010	1013	1007	1009	1010	1013	1008	1004	1006	1006
E_{2g}		1					442	446	443					437	444	447
															913	914
	H_2O II		3595	3595	3594	3597	3597	3598	3598	3597	3594	3598	3596	3595		
	H_2O I		3607	3606	3604	3606	3607	3606	3607	3606	3607	3606	3607	3606	3606	3606

List of references: 1 – Adams & Gardner (1974); 2 – Charoy et al. (1996); 3 – Hagemann et al. (1990)

Tab. 3. Content of selected chromophores in the studied samples determined by μXRF (in oxides wt %).

	B1	B2	B3	B4	B5	B6	B7	B8	B9	B10	B11	B12	B13	B14
Cr_2O_3	0.46	0.15	0.23	0.89	0.15	0.00	1.57	0.61	0.02	0.76	0.25	0.25	0.83	0.92
V_2O_3	0.04	0.24	0.11	0.02	0.00	0.05	2.15	0.77	0.06	0.13	0.09	0.09	0.03	0.00
FeO	2.96	2.86	1.38	1.07	1.12	3.11	0.21	0.07	0.59	4.21	0.66	2.31	5.30	6.73
NiO	0.07	0.03	0.02	0.00	0.03	0.01	0.03	0.03	0.00	0.00	0.00	0.00	0.45	0.44
CuO	0.03	0.00	0.01	0.02	0.02	0.03	0.00	0.01	0.05	0.02	0.03	0.03	3.36	5.06

is overlapping with Fe^{2+} absorption band at 635-648 nm. The third narrow absorption band attributed to the spin-forbidden $^4A_{2g} \rightarrow {}^2T_{1g}$ transition in Cr^{3+} cation displays at 683-684 nm. The Fe^{2+} absorption band is similar in all three samples. Main absorption bands in these samples are not overlapping which results in strong transmission in green region at 500-510 nm and weaker transmission in the red to NIR region at 680-720 nm. This transmission produces the typical emerald green colour of these samples.

In contrast, the second group of samples – B2–B5 (Fig. 10) B10 (Fig. 11) have a more or less different hue to the emerald-green colour. These samples has relatively distinctive band at 428-435 nm assigned to dominant $^4A_{2g} \rightarrow {}^4T_{2g}$ transition in Cr^{3+}. The second Cr^{3+} band at 603-610 nm but it is also overlapping with Fe^{2+} absorption band at 640-645 nm. The third narrow Cr^{3+} absorption band cation is at 682-686 nm. The Fe^{2+} absorption band is similar in all three samples but varies in intensity. All samples in the second group have weaker transmission in the green region and usually less pronounced transmission in the red to NIR region (except B4 sample) than samples from the first group.

The third group including B6 (Fig. 10), B9 (Fig. 11) displays no significant bands between 500-700 nm indicating Cr absence. The only bands are attributed to Fe. The wide transmission area results in grass-green coloured beryl.

The B13 and B14 samples (Fig. 12) share some properties with the first two groups. Similarly to the first group, these have strong transmission in the green region at 500-510 nm bordered by the

Tab. 4. Wavelength (in nm) of the absorption bands in the studied samples.

Sample	B1	B2	B3	B4	B5	B6	B7
Fe^{3+}		406	406			403	
Cr^{3+} (V^{3+})	432	428	435	434	430		437
Cr^{3+} (V^{3+})	605	603	607	604	609		614
Fe^{2+}	635	640	643	649	643		
Cr^{3+}	684	686	683	682	683		682
Fe^{2+}	835	841	837	834	830	826	
Cu^{2+}							
Sample	**B8**	**B9**	**B10**	**B11**	**B12**	**B13**	**B14**
Fe^{3+}		432					
Cr^{3+} (V^{3+})	437		426	427	429	430	424
Cr^{3+} (V^{3+})	616		610	614	616	607	606
Fe^{2+}			645	645	648	645	652
Cr^{3+}	682		683	683	683		685
Fe^{2+}		823	851	840	840		759
Cu^{2+}							907

Cr^{3+} bands at 424-430 and 606-607 nm. However, B13 and B14 have no transmission in the red to NIR region due to high Fe^{2+} absorption. Moreover, B14 sample displays Cu^{2+} absorption at 907 nm which is missing in B1-B12 samples and in B13 sample NIR region was unresolvable.

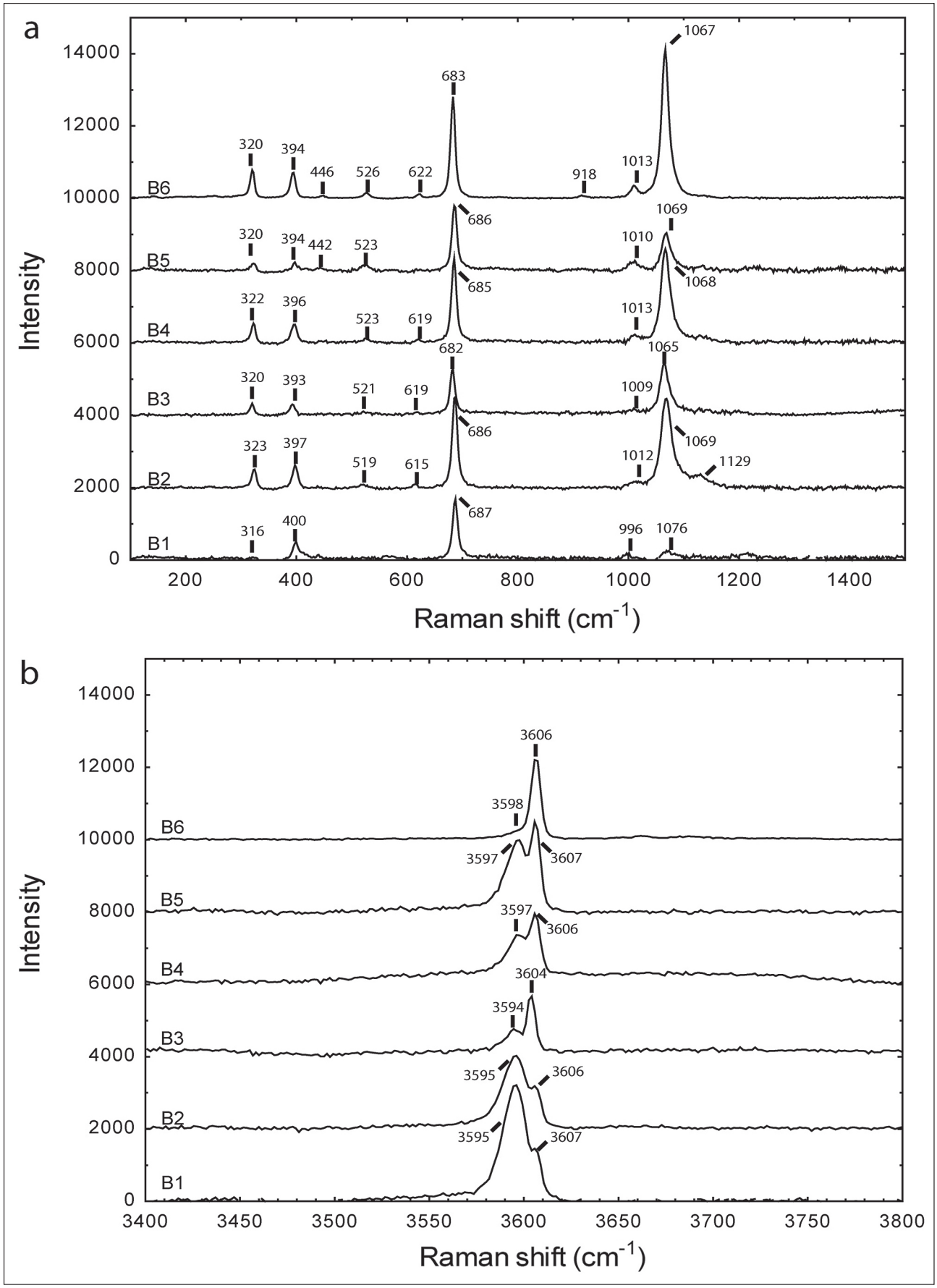

Fig. 3. Raman spectra of the studied samples.

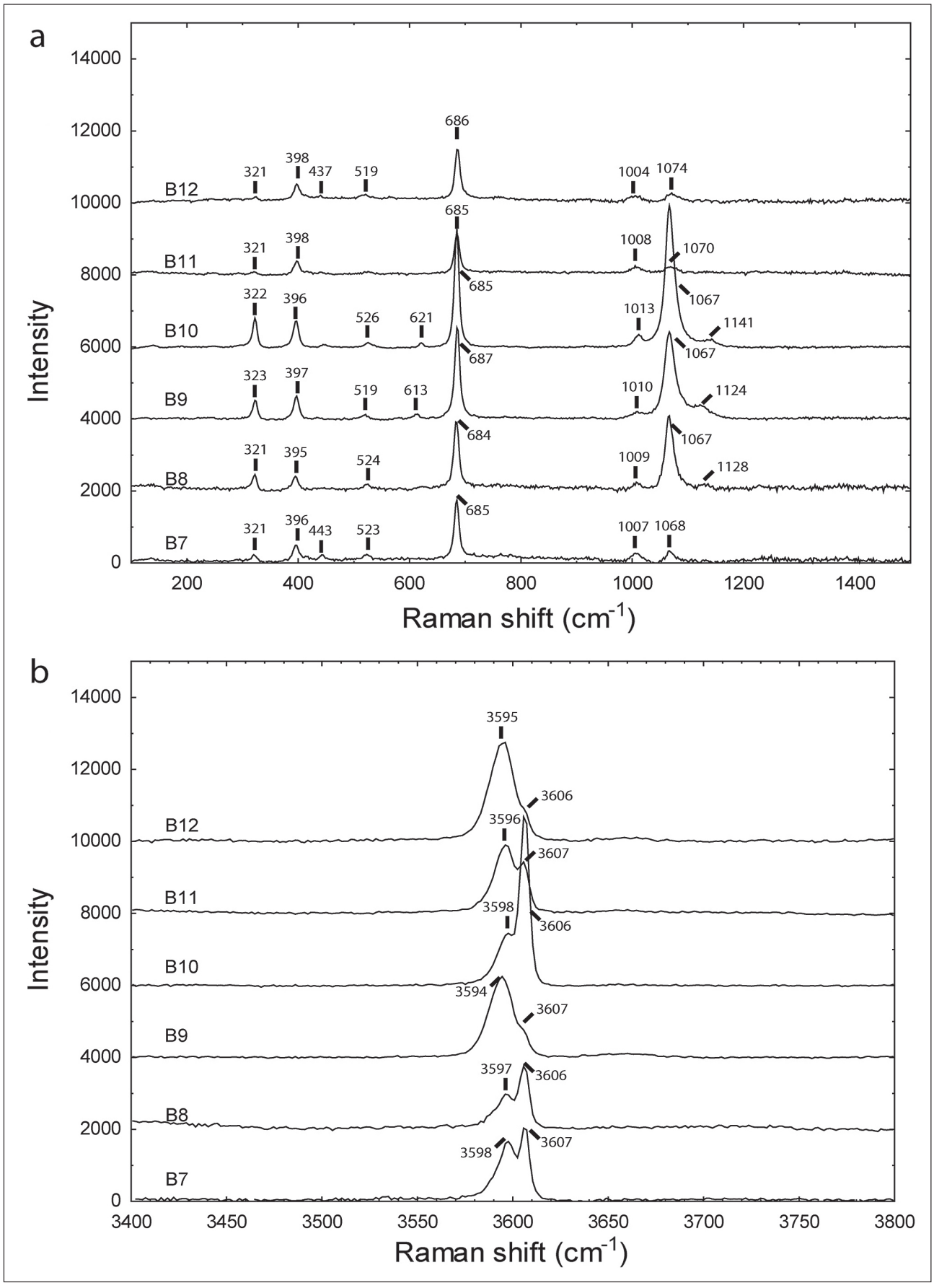

Fig. 4. Raman spectra of the studied samples.

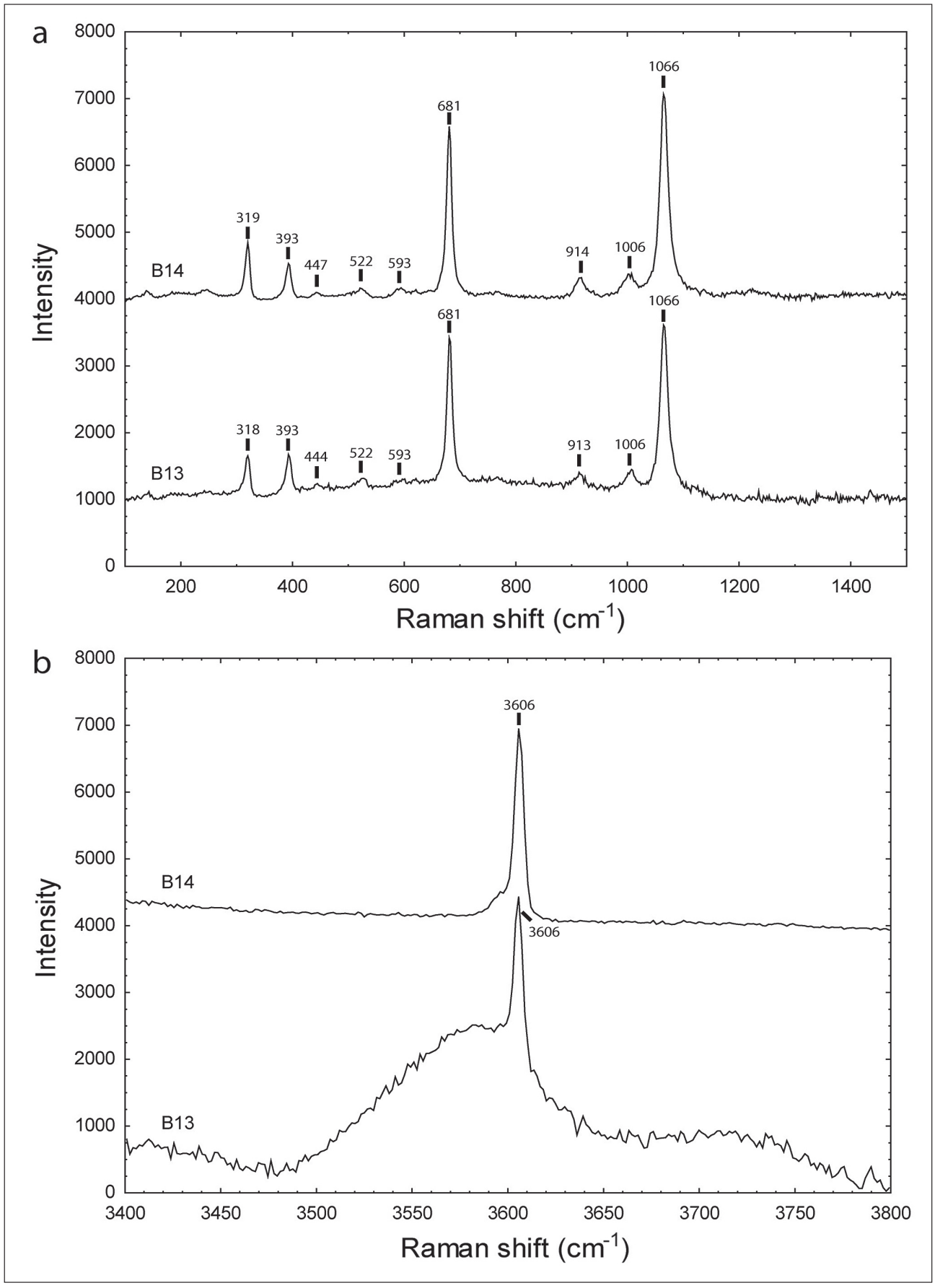

Fig. 5. Raman spectra of the studied samples.

The last group includes B7 and B8 samples (Fig. 11) with the absorption spectra the most characteristic for emerald. The emerald-green colour from the intensive transmission in the green region at 510 nm results from the strong absorption at 437 nm and 614-616 nm bands. These can be attributed to both Cr^{3+} and V^{3+} which are enriched in these samples. Low absorption in red to NIR region (740-1000 nm) reflects the negligible Fe content in these samples.

4. DISCUSSION

4.1. Identification of sample origin

A Raman investigation allowed the identification of 14 beryl samples and, moreover, the XRF chemical study demonstrated their variable origin. Most of world emerald occurrences are in the FeO-Cr_2O_3 trend, only B7 and B8 samples are significantly

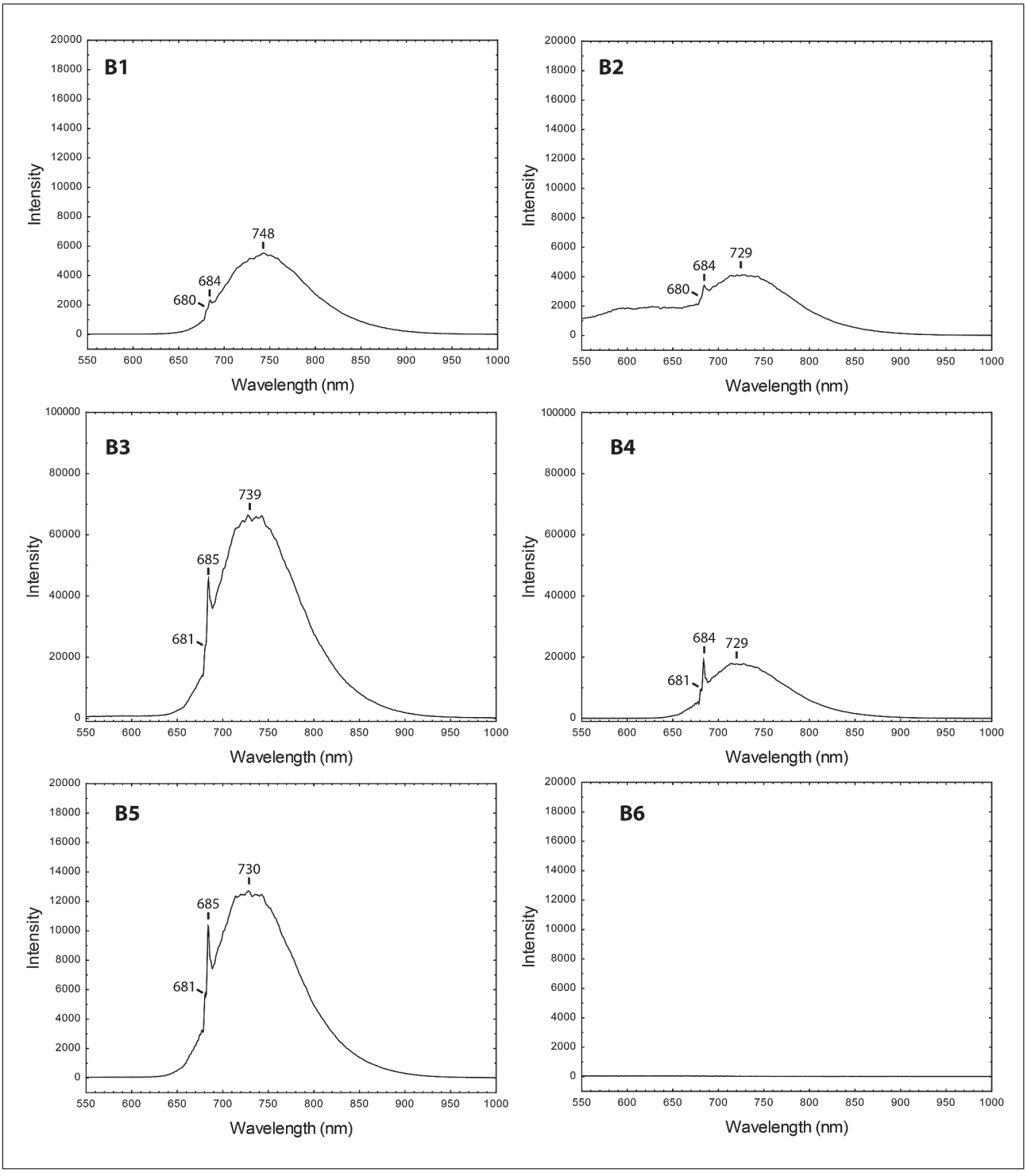

Fig. 6. Luminescence spectra of the studied samples.

enriched in V_2O_3 and poor in FeO (Fig. 9). Moreover, emerald from Norway is V-dominant with a negligible Fe and Cr content (Groat et al., 2008), therefore, this origin is unlikely for B7, B8 samples. In our samples, the majority is in line with the general FeO-Cr_2O_3 trend. The B7 and B8 samples fell into the field of published analyses from Colombia (Groat et al., 2008). Based on the chemical composition, the origin of the B1-B12 samples declared by retailer seems to be likely.

Optical microscopy is also an essential tool to distinguish different sources of green-coloured beryl. The most valuable Colombian emeralds are typical by three-phase inclusions although recently, other sources of emerald (e.g., in China, Davdar locality; in Zambia, Musakashi area) with similar inclusions were found (Saeseaw et al. 2014; Pardieu et al. 2015). Only B7, B8 samples, which were declared as Colombian emeralds by retailer, manifested the three-phase inclusions presence. Other studied

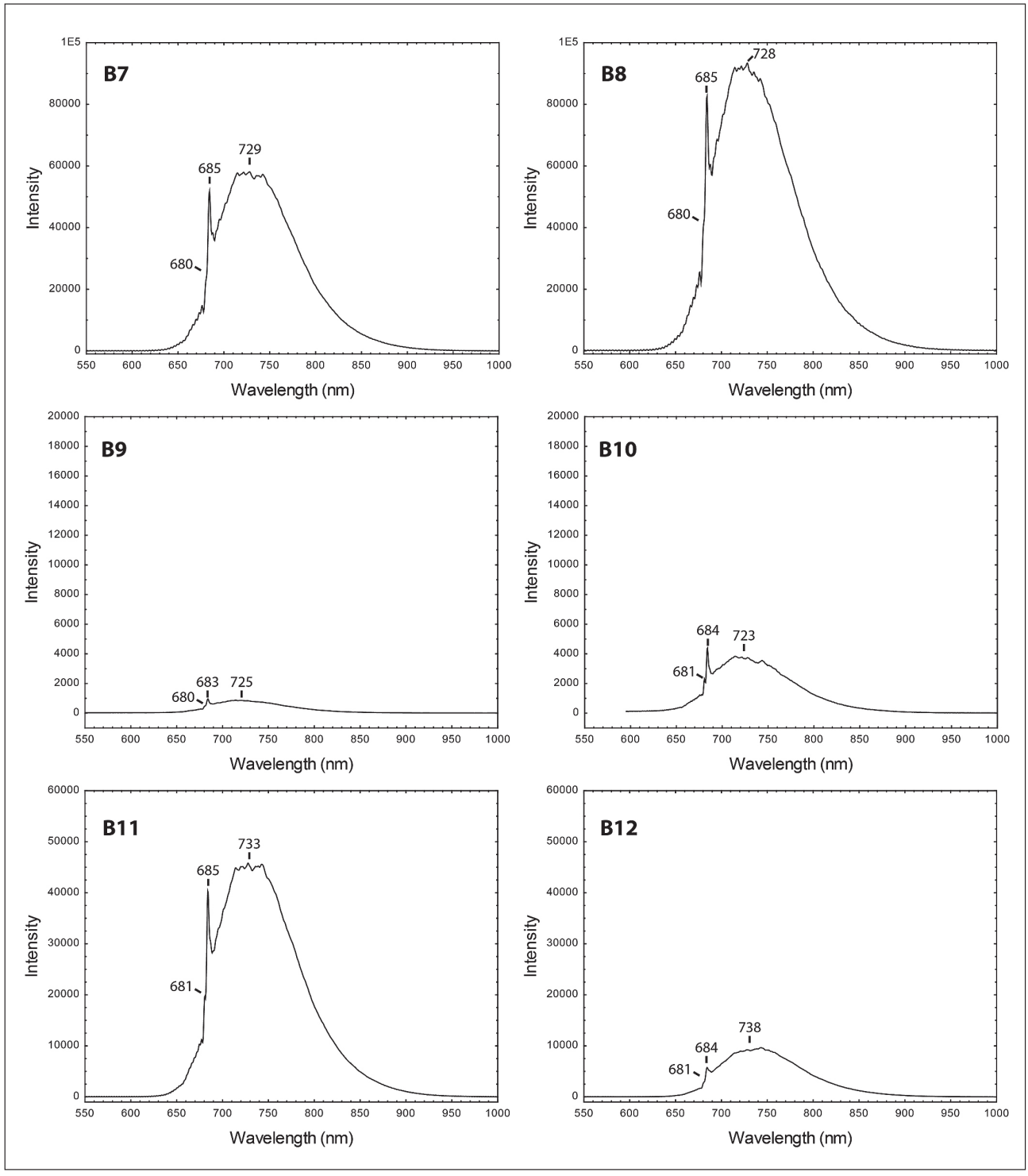

Fig. 7. Luminescence spectra of the studied samples.

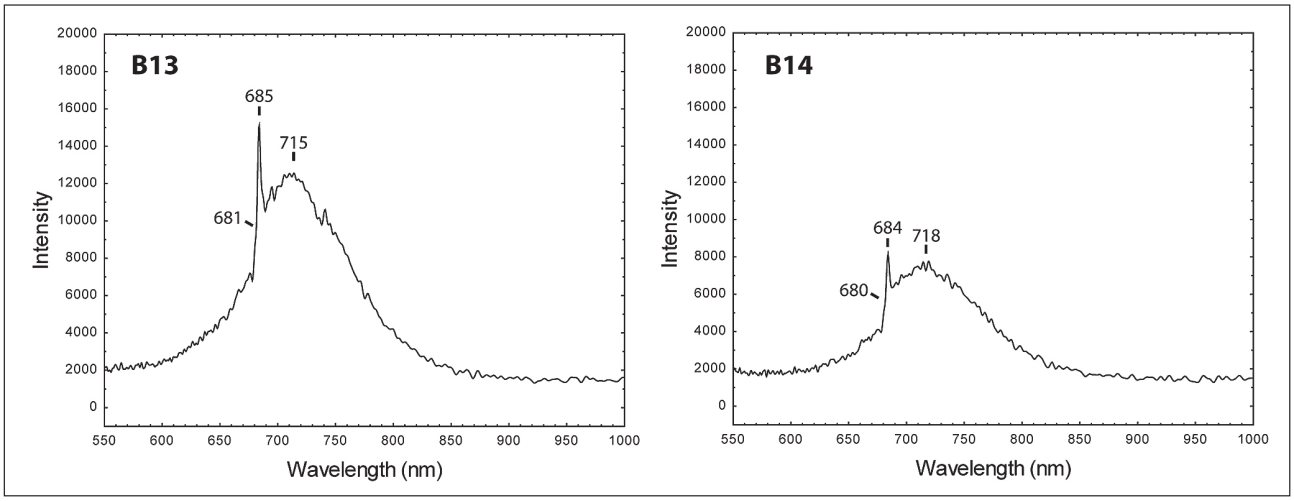

Fig. 8. Luminescence spectra of the studied samples.

samples had only two-phase inclusions. Therefore, the inclusions nature in these samples is not sufficient identification factor to determine exact source or origin. Flux patterns presence in the B14 sample is a good indicator of synthetic origin (Shelementiev & Serov, 2011).

For natural emerald origin, schist and non-schist type is often used to indicate the host rocks and genesis (Moroz et al., 2000; Groat et al., 2008; Huong & Häger, 2010). Emeralds can commonly be found in metamorphic basic and ultrabasic rocks associated with granite and pegmatite intrusions – schist type – but also in the sedimentary-derived black shales with signs of hydrothermal activity – non-schist type (Moroz et al., 2000; Groat et al., 2008). This classification can distinguish high-alkali (schist type) from low-alkali emeralds (non-schist type) (Bersani et al., 2014). The relatively higher Fe content in B1-B6, B9-B12 samples which is indicative of an octahedral substitution and therefore, increased alkali content (Aurisicchio et al., 1988), suggests schist origin. Only B7 and B8 samples with a dominant Cr and V for Al substitution are probably of (Colombian) non-schist origin.

The alkali content can be indicated by the presence of the H_2O type. Water is present in the channel site but involves two different orientations. Water type I is associated with lack of alkali ions, and its molecular two-fold axis is oriented perpendicular to the six-fold *c* axis of beryl. Type II H_2O is connected with alkali, and its two-fold axis is oriented parallel to the six-fold *c* axis of beryl (Wood & Nassau, 1967, 1968; Aurisicchio et al., 1994; Charoy et al., 1996; Kolesov & Geiger, 2000; Łodziński et al., 2005; Kolesov, 2008). Water band intensities approximately corresponded with type classification; emeralds with relatively significant Raman band at 3594-3598 cm^{-1} indicating alkali enrichment (Fridrichová et al., 2016) include B1-B5 and B10-12 samples. In contrast, alkali poor emeralds with minute band for H_2O type II involve B6-B9.

The B13 and B14 samples are most likely syntheses due to a synthetic tester result and the Cu and Ni presence, which is consistent with data on Russian synthetic emeralds (Mashkovtsev & Smirnov, 2004). Both samples contain only water type I, whereas Huong & Häger (2010) suggest that two types of water can be

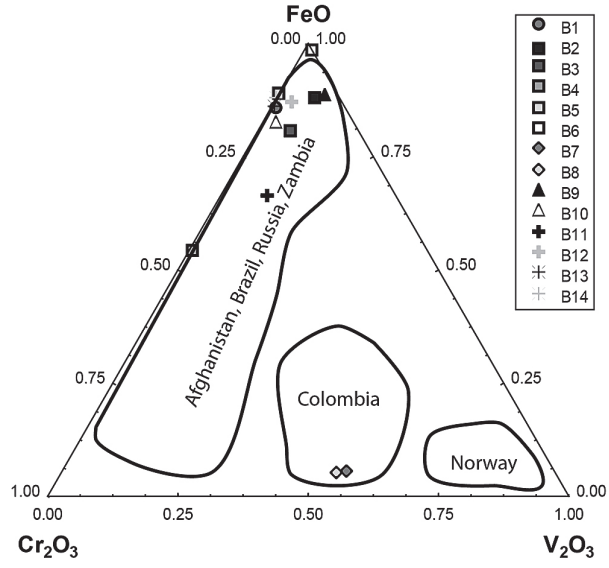

Fig. 9. Triangular FeO-Cr_2O_3-V_2O_3 diagram of the studied samples. The shown areas demonstrate emerald compositions of different localities (Groat et al. 2008)

associated only with natural samples. Our observation supports therefore the possibility of the synthetic origin.

Emeralds can be synthetized by two methods: hydrothermal and flux-grown (Nassau, 1980; Barilo et al., 1999). Water presence in synthetic emerald is a hydrothermal origin evidence because flux-grown process is water-free (Nassau, 1980). In general, hydrothermal synthetic emeralds can contain variable alkali proportion (Shelementiev & Serov, 2011). Biron and Tairus hydrothermal synthetic emeralds analysed by Huong et al., 2014 are relatively alkali-poor (total alkali up to 0.166 wt %) and only water type I was detected in these samples. Unusual chromophores such as Ni and Cu and water in our B13 and B14 samples confirm the synthetic hydrothermal origin. Moreover, we can presume that our studied synthetic emeralds are from a Russian production, due to the Cr, Fe, Cu, Ni presence and

V, Cl absence (Mashkovtsev & Smirnov, 2004; Mashkovtsev & Solntsev, 2002). We can exclude Linde-Regency, Biron and Malossi syntheses containing Cl but no Ni or Cu (Adamo et al., 2005).

4.2. Chromophores and luminophores

Green beryl colour can be caused by Cr^{3+}, V^{3+} and Fe^{2+} and Fe^{3+} (Wood & Nassau, 1968). However, only beryl which contains sufficient Cr^{3+} and/or V^{3+} to produce a strong green colour, which should be termed emerald. Vanadium as the chromophore also produces emerald-like colour and Cr-rich emeralds usually show sufficient vanadium content, therefore, the origin of their colour can be attributed to both chromium and vanadium (Wood & Nassau, 1968). Schwarz & Schmetzer (2002) defined emerald as yellow green, green or blue green natural or synthetic beryl which exhibits obvious Cr and/or V absorption bands in red and blue-violet region of optical spectra. Both natural or synthetic

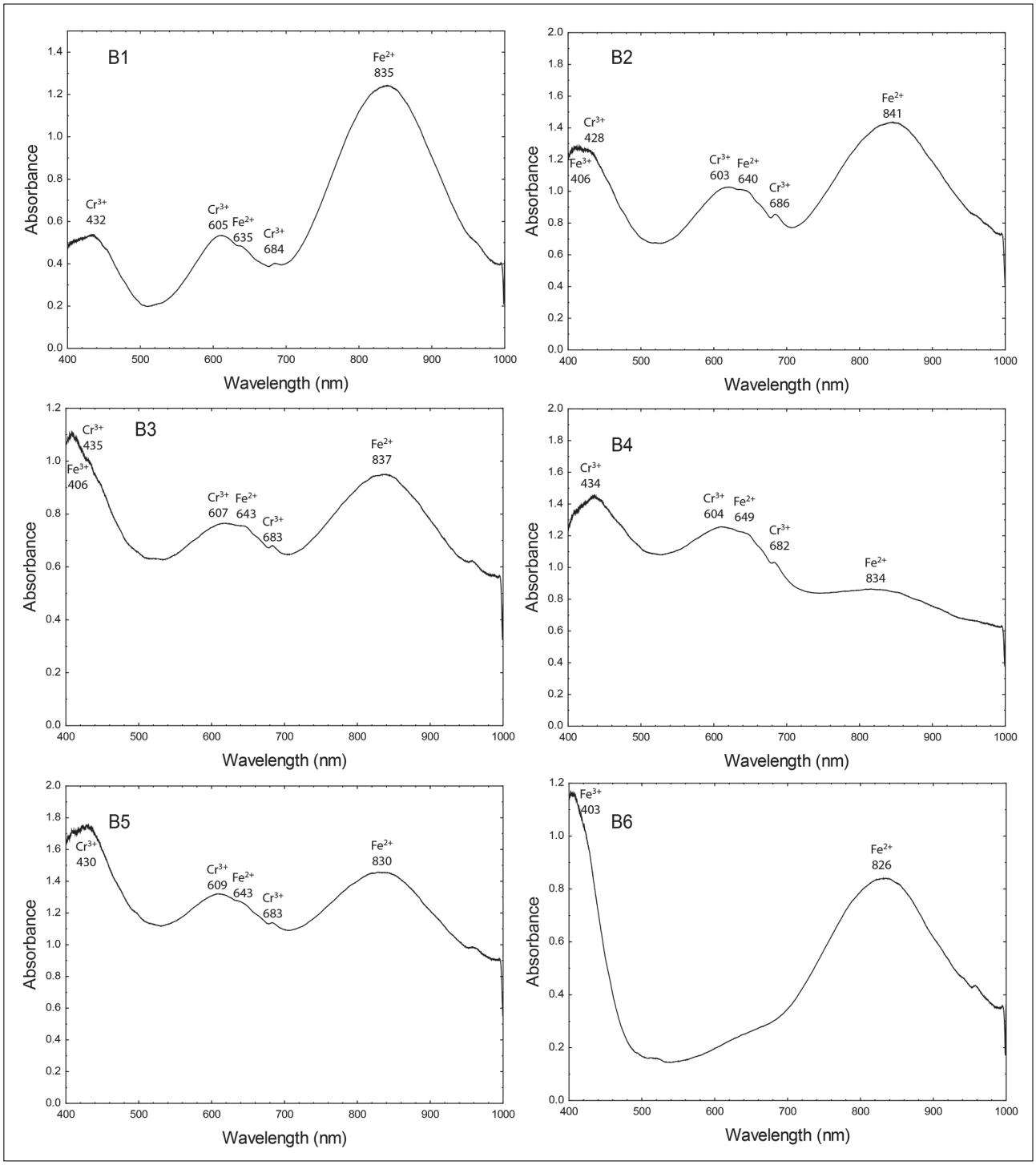

Fig. 10. Optical spectra of the studied samples.

(flux-grown or hydrothermal) emeralds exhibit the same two broad bands near 430 and 600 nm as sharp lines at low temperatures for Cr^{3+} (Wood, 1965); one in the blue at 476 and two in the red at 680 and 683 nm.

Colombian emeralds are the most desirable green stones, because of their unique rich-green colour, caused by high chromium and vanadium content which was also observed in our B7 and B8 samples. The gemmological quality increases with Cr and/or V content, therefore, B1, B4, B7, B8, B11, B12 samples have typical emerald-green colour. In contrast, Fe-rich stones (B2-B6, B9, B10 samples) are typically grass-green.

Green stones which do not contain Cr should be named as green beryl; they are less valuable than emeralds. Green beryl coloured by Fe may contain Fe^{3+} in octahedron and Fe^{2+} in channel (Nassau, 1999) or Fe^{2+} in octahedron and the part of Fe^{3+} in the tetrahedron (Andersson, 2013; Fridrichová et al., 2018). Green colour in such beryl results from absorption in yellow-orange to red region between 610 and 810 nm (Fe^{2+})

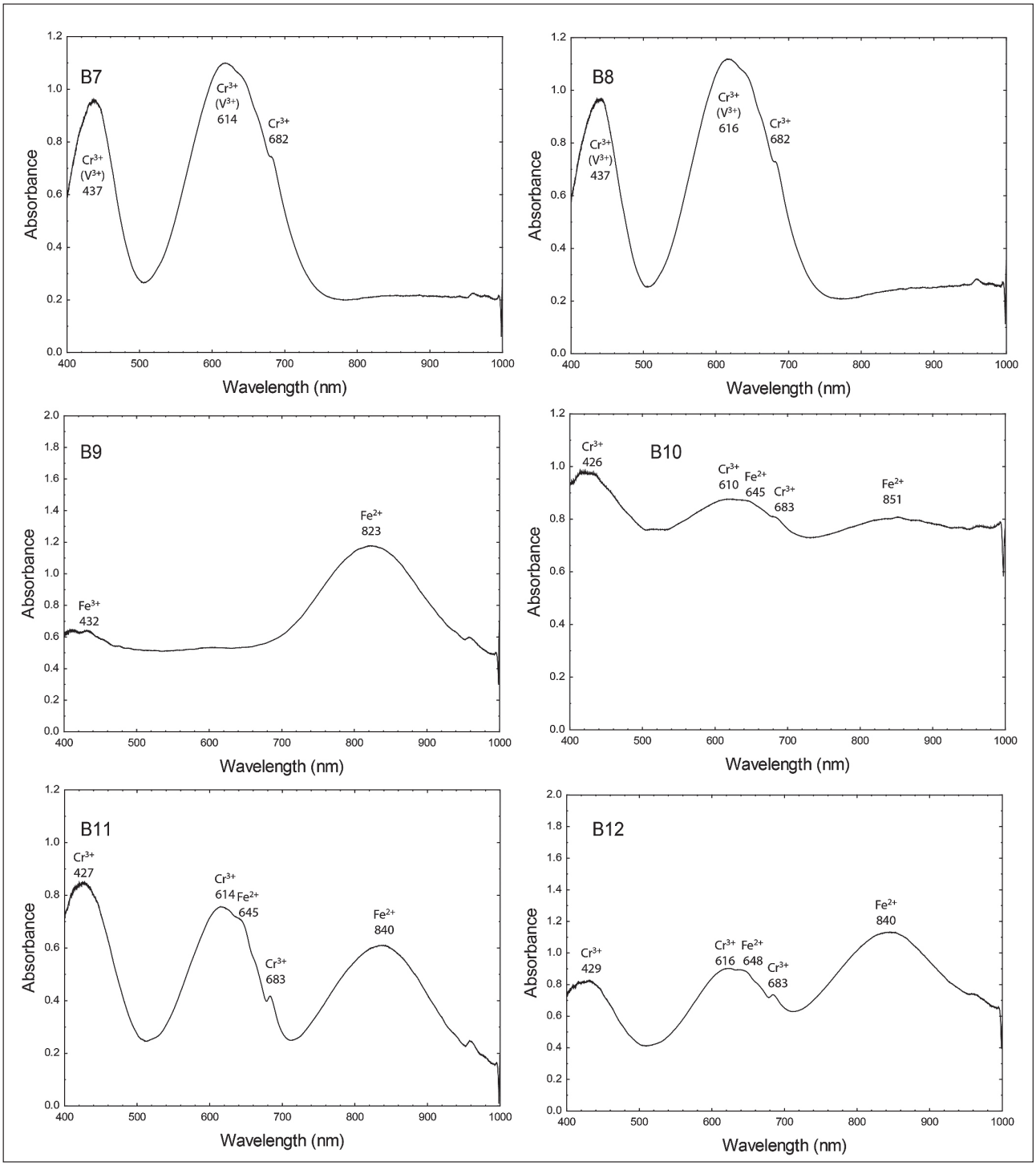

Fig. 11. Optical spectra of the studied samples.

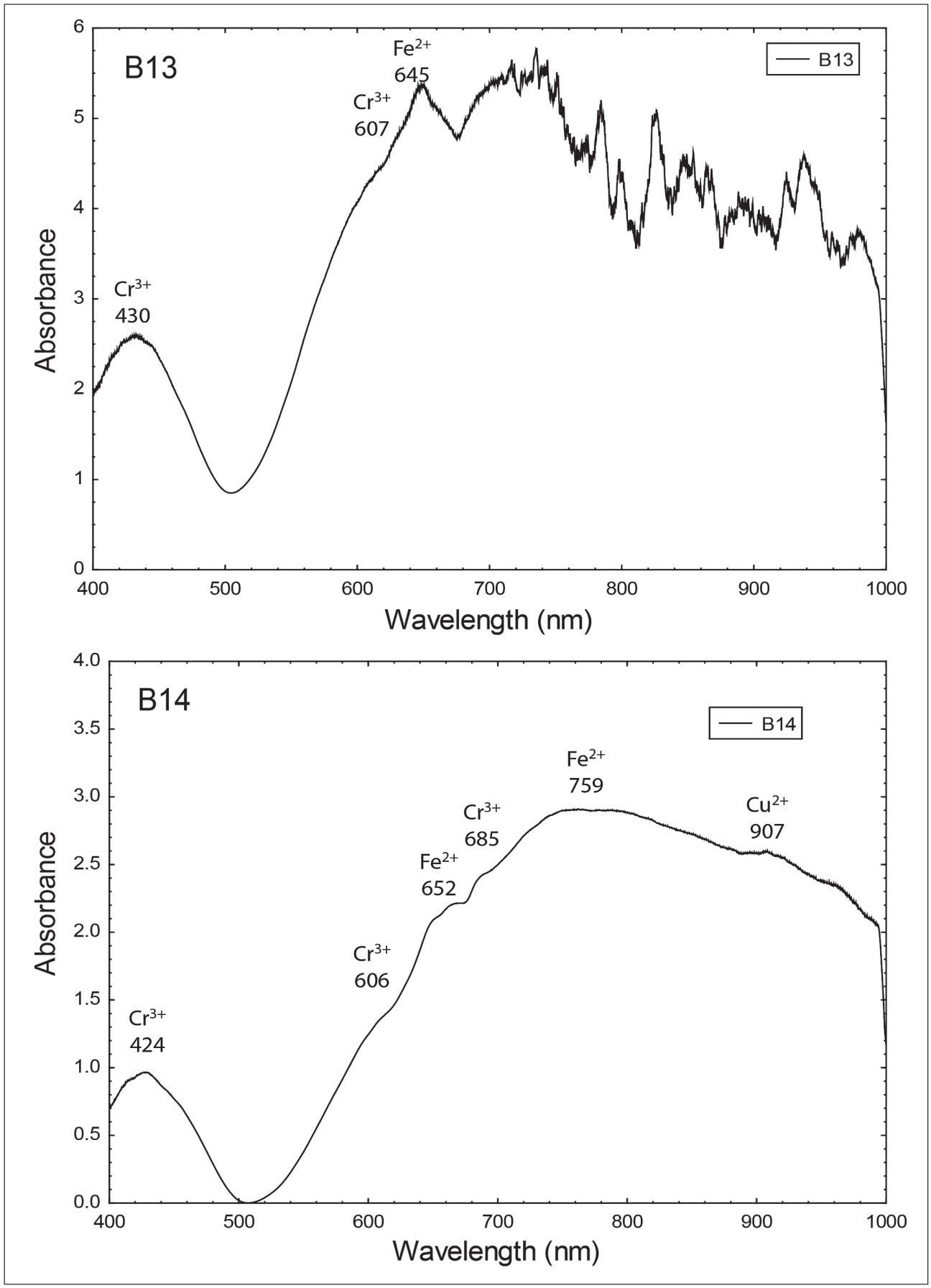

Fig. 12. Optical spectra of the studied samples.

with green transmission (Wood & Nassau, 1968). However, the transmission partly extends to yellow region which results in grass-green colour due to the yellow hue. Only the B6 and B9 samples can be reliably marked as green beryl; these are Fe-enriched but Cr and V contents are near or below XRF detection limit. Their grass-green colour is less saturated compared to the other samples and also significantly differs from them in tone and hue.

A few samples, mainly B3, B7, B8 and B11, exhibited high luminescence intensity. Chromium is the main luminophore (Gaft et al., 2015), which is manifested by two narrow lines between 680 and 685 nm that arise from electronic decay of a doublet metastable state (Wood, 1965) and are known as *R* lines. The longer-wavelength line is denoted R_1 and the shorter-wavelength is R_2 (Carceller-Pastor et al., 2013). Broad band centred at about 720 nm could be assigned to Fe^{3+} which is consistent by published data (Bersani et al., 2014). These bands are present in the most of the studied samples spectra except B6 (absent luminescence) and B9 (very low luminescence). These samples had the lowest Cr content. Therefore, Cr luminescence is the very important identification factor for emeralds. It allows recognizing emerald from green beryl with Raman spectroscopy in absence of other spectroscopic (chemical) data.

5. CONCLUSIONS

Based on the microscopic observations and spectroscopic data, it was possible to partly identify the studied samples origin.

All the samples were identified as beryl by Raman spectroscopy and all except B6 and B9 samples can be termed as emerald coloured by Cr^{3+} and V^{3+}. The Cr presence was confirmed by XRF and optical absorption spectroscopy, but also R_1 and R_2 luminescence features in Raman spectra. These luminescence features are very useful in emerald identification without using chemical analysis. The B6 and B9 samples are green beryl due to very low content of Cr and V and Fe presence as the main chromophore.

The B7 and B8 samples can be confirmed as natural Colombian non-schist emeralds due to Cr, V and Fe ratio and three-phase inclusions presence.

The B1-B6 and B9-B12 samples are natural schist-type emerald and green beryl, because of higher Fe content indicating octahedral substitution which involves higher alkali content. Exact localization cannot be estimated based on the current data, but nothing excluded declared stone origin.

The B13 and B14 samples are very likely of synthetic hydrothermal probably Russian origin. This is evidenced by microscopic flux patterns, Cu, Ni and H_2O presence.

The microscopic and spectroscopic study is very useful to generally distinguish green-coloured beryl origin. However, exact determination of beryl origin to country or even locality requires advanced analytical methods (trace elements and isotopes analysis).

Acknowledgments: The authors thank Andreas Ertl and Simone Ferreira da Silva for their detailed reviews and very useful suggestions.

References

Adamo I., Pavese A., Prosperi L., Diella V., Merlini M., Gemmi M. & Ajò D., 2005: Characterization of the new Malossi hydrothermal synthetic emerald. *Gems & Gemology*, 41, 4, 328–338.

Adams D. M. & Gardner I. R., 1974: Single-crystal vibrational spectra of beryl and dioptase. *Journal of the Chemical Society - Dalton Transactions*, 14, 1502–1505.

Andersson L. O., 2013: The yellow color center and trapped electrons in beryl. *Canadian Mineralogist*, 51, 1, 15–25.

Aurisicchio C., Fioravanti G., Grubessi O. & Zanazzi P.F., 1988: Reappraisal of the crystal chemistry of beryl. *American Mineralogist*, 73, 7–8, 826–837.

Aurisicchio C., Grubessi O. & Zecchini P., 1994: Infrared spectroscopy and crystal chemistry of the beryl group. *Canadian Mineralogist*, 32, 1, 55–68.

Barilo S. N., Bychkov G. L., Kurnevich L. A., Leonuk N. I., Mikhailov V. P., Shiryaev S. V., Koyava V. T. & Smirnova T. V., 1999: Controlled crystallization of emerald from the fluxed melt. *Journal of Crystal Growth*, 198–199, Part I, 716–722.

Bersani D., Azzi G., Lambruschi E., Barone G., Mazzoleni P., Raneri S., Longobardo U. & Lottici P. P., 2014: Characterization of emeralds by micro-Raman spectroscopy. *Journal of Raman Spectroscopy*, 45, 11–12, 1293–1300.

Carceller-Pastor I., Hutchinson W. D. & Riesen H., 2013: Temperature dependence of the chromium (III) R_1 linewidth in emerald. *Chemical Physics Letters*, 564, 33–36.

Charoy B., De Donato P., Barres O. & Pinto-Coelho C., 1996: Channel occupancy in an alkali-poor beryl from Serra Branca (Goias, Brazil): Spectroscopic characterization. *American Mineralogist*, 81, 3–4 395–403.

Fridrichová J., Bačík P., Bizovská V., Libowitzky E., Škoda R., Uher P., Ozdín D. & Števko M., 2016: Spectroscopic and bond-topological investigation of interstitial volatiles in beryl from Slovakia. *Physics and Chemistry of Minerals*, 43, 6, 419–437.

Fridrichová J., Bačík P., Ertl A., Wildner M. & Miglierini M., 2018: Crystal chemistry and Jahn-Teller distortion of Mn^{3+}-occupied octahedra in red beryl from Utah. *Journal of Molecular Structure*, 1152, 79–86.

Gaft M., Reisfeld R. & Panczer, G., 2015: Modern Luminescence spectroscopy of Minerals and Materials. Springer Cham Heidelberg New York Dordrecht London, Second edition, 606 p.

Giuliani G., France-Lanord C., Coget P., Schwarz D., Cheilletz A., Branquet Y., Giard D., Martin-Izard A., Alexandrov P. & Piat D. H., 1998: Oxygen isotope systematics of emerald: relevance for its origin and geological significance. *Mineralium Deposita*, 33, 5, 513–519.

Groat L. A., Giuliani, G., Marshall D. D. & Turner D., 2008: Emerald deposits and occurrences: A review. *Ore Geology Reviews*, 34, 1–2, 87–112.

Hagemann A., Lucken A., Bill H., Gysler-Sanz J. & Stalder H. A., 1990: Polarized Raman spectra of beryl and bazzite. *Physics and Chemistry of Minerals*, 17, 5, 395–401.

Huong L. T. T. & Häger T., 2010: On some controversially-discussed Raman and IR bands of beryl. *VNU Journal of Science, Earth Sciences*, 26, 1, 32–41.

Huong L. T. T., Hofmeister W., Häger T., Karampelas S. & Kien N. D.-T., 2014: A preliminary study on the separation of natural and synthetic emeralds using vibrational spectroscopy. *Gems & Gemology*, 50, 4, 287–292.

Kolesov B., 2008: Vibrational States of H_2O in beryl: Physical aspects. *Physics and Chemistry of Minerals*, 35, 5, 271–278.

Kolesov B. A. & Geiger C. A. 2000: The orientation and vibrational states of H_2O in synthetic alkali-free beryl. *Physics and Chemistry of Minerals*, 27, 8, 557–564.

Łodziński M., Sitarz M., Stec K., Kozanecki M., Fojud Z. & Jurga S., 2005: ICP, IR, Raman, NMR investigations of beryls from pegmatites of the Sudety Mts. *Journal of Molecular Structure*, 744–747, 1005–1015.

Mashkovtsev R. I. & Solntsev V. P., 2002: Channel constituents in synthetic beryl: ammonium. *Physics and Chemistry of Minerals*, 29, 1, 65–71.

Mashkovtsev R. I. & Smirnov S. Z., 2004: The nature of channel constituents in hydrothermal synthetic emerald. *Journal of Gemmology*, 29, 4, 215–227.

Moroz I., Roth M., Boudeulle M. & Panczer G., 2000: Raman microspectroscopy and fluorescence of emeralds from various deposits. *Journal of Raman Spectroscopy*, 31, 6, 485–490.

Nassau K., 1980: Gems made by man. Chilton, Radnor, 364 p.

Nassau K., 1999: Gemstone enhancement: history, science and state of the art. St. Edmundsbury Press Ltd., Manchester, 252 p.

Pardieu V., Detroyat S., Sangsawong S. & Saeseaw S. 2015: Tracking emeralds from the Musakashi area of Zambia. *InColor*, 29, 18-25.

Saeseaw S., Pardieu V. & Sangsawong S., 2014: Three-phase inclusions in emerald and their impact on origin determination. *Gems and Gemology*, 50, 2, 114–132.

Schwarz D. 1991: Die chemischen Eigenschaften der Smaragde, II. Australien und Norwegen [Chemical properties of emerald, II. Australia and Norway]. *Zeitung der Deutschen Gemmologischen Gesellschaft*, 40, 39–66. [in German].

Schwarz D. & Schmetzer K., 2002: The Definition of Emerald: The green variety of beryl colored by chromium and/or vanadium. *In*: Giuliani et al., (Eds.): Emeralds of the World ExtraLapis English, 2, 74–78.

Shelementiev Y. & Serov R., 2011: Synthetic emeralds MSU Gemmological Centre of Moscow University. *Annual CIBJO Congress Emerald Day Conference*.

Stockton C. M., 1987: The separation of natural from synthetic emeralds by infrared spectroscopy. *Gems & Gemology*, 23, 2, 96–99.

Wood D. L., 1965: Absorption fluorescence and Zeeman effect in emerald. *Journal of Chemical Physics*, 42, 10, 3404–3410.

Wood D. L. & Nassau K., 1967: Infrared spectra of foreign molecules in beryl. *Journal of Chemical Physics*, 47, 7, 2220–2228.

Wood D. L. & Nassau K., 1968: The characterization of beryl and emerald by visible and infrared absorption spectroscopy. *American Mineralogist*, 53, 5–6, 777–800.